A Framework for Outdoor RGB Image Enhancement and Dehazing

Alina Majeed Chaudhry, Muhammad Mohsin Riaz, and Abdul Ghafoor

***Abstract*— A framework for image visibility restoration and haze removal is proposed. The proposed technique utilizes hybrid median filtering in conjunction with accelerated local Laplacian filtering for initial dehazing of images. For visual enhancement and correct restoration of colors, constrained l_0-based gradient image decomposition is applied. The proposed technique not only effectively removes haze from the images but also addresses the issues of distorted colors, visual, and halo artifacts, and haze removal from sky region in images in a better way when compared to other techniques. Experiments were performed on outdoor RGB images as well as remotely sensed images. The effectiveness of our proposed technique is demonstrated by quantitative and visual analyzes.**

***Index Terms*— Accelerated local Laplacian filter, haze removal, visibility restoration.**

I. Introduction

WHEN images are captured in an outdoor environment, they may suffer from low contrast, poor visibility, dark, and inconsistent colors due to the presence of haze or fog. Haze removal from such images is an important requirement for computational photography as well as several computer vision tasks (analysis of a scene, biometrics, tracking of targets, remote sensing, and surveillance). In contrast to classical dehazing, which requires depth information, the state of the art techniques consider haze removal as an ill-posed problem-nonavailability of depth information. Some dehazing techniques require several images which are captured under varying light or climatic conditions. Graphical model using scene albedo [1] requires additional statistical information for dehazing.

Image dehazing using dark channel prior (DCP) [2] is computationally complex and suffers from visual artifacts. A haze removal technique based on brightness and saturation ratio [3] has a high computational cost. Edge-guided interpolation-based technique [4] removes dense fog but is computationally complex. Regularization-based haze removal [5] generates halo artifacts in large sky regions. Optimal transmission map-based image dehazing [6] provides visually appealing results at the cost of computational complexity. Similar to the method in [8], which does not effectively remove haze from images with strong haze gradients. A technique based on contrast enhancement [9] uses dehazing for image matching using local features. An algorithm for haze detection effectively removes haze [10] and cirrus from remotely sensed multispectral imagery [11]. Recently, a multispectral data set has been presented for assessing the performance of dehazing algorithms [12]. A fast dehazing method is based on the existence of a linear relationship in the minimum channel between the hazy and the haze-free image [13]. A recent method for haze removal is based on the perception-oriented optical transmission estimation [14]. Entropy-dependent contextual regularization and quad-tree decomposition-based image dehazing [15] effectively removes haze but sometimes provides limited performance in the case of dense fog or large sky regions. A new technique for haze removal reduces the color distortion problem by redefining the visibility restoration model and uses modified gain intervention filter based-DCP approach for refining the estimated coarse atmospheric veil [16]. Another recent technique uses a modified joint trilateral filter-based DCP approach for enhancing the estimated coarse air veil and redefines the estimated transmission map for dehazing of remotely sensed images [17]. An algorithm for haze removal makes use of multiscale products of the image as a prior. The hazy image is decomposed in approximation and details subbands through the Laplacian decomposition, and the approximation subbands of each level are multiplied in order to obtain the multiscale products of each band, which are summed up, and the l_{th} root is calculated for obtaining this prior [18]. A technique based on modified retinex algorithm employs color restoration and atmospheric light scattering physical model for haze removal [19]. Dehazing based on DCP and Gaussian filtering [8] provides limited accuracy in the case of images having large haze gradient. A haze removal technique for satellite images based on linear intensity transform [20] fails to distinguish between large scale grounds and dense haze.

In this letter, a framework for single image enhancement and haze removal making use of image filtering, and detail enhancement is proposed. The partial visibility of the image is restored by inferring the atmospheric veil using hybrid median filtering. Accelerated local Laplacian filtering is applied to the grayscale version of the image. This step significantly removes haze, and also preserves edges and minimizes visual artifacts in the image. This filter is quite fast and has a linear time complexity. The local Laplacian filtered image and the image with partial restored visibility are blended to obtain a resultant image. The local Laplacian filtered image may have low brightness and a few dark regions, which are expected to be well lit in the original image; therefore, further processing

Manuscript received September 19, 2017; revised January 28, 2018; accepted February 10, 2018. Date of publication April 5, 2018; date of current version May 21, 2018. *(Corresponding author: Abdul Ghafoor.)*

A. M. Chaudhry and A. Ghafoor are with the National University of Sciences and Technology, Islamabad 44000, Pakistan (e-mail: alina.phd@students.mcs.edu.pk; abdulghafoor-mcs@nust.edu.pk).

M. M. Riaz is with CAST, COMSATS Institute of Information Technology, Islamabad 45550, Pakistan (e-mail: mohsin.riaz@comsats.edu.pk).

Color versions of one or more of the figures in this letter are available online at http://ieeexplore.ieee.org.

Digital Object Identifier 10.1109/LGRS.2018.2814016

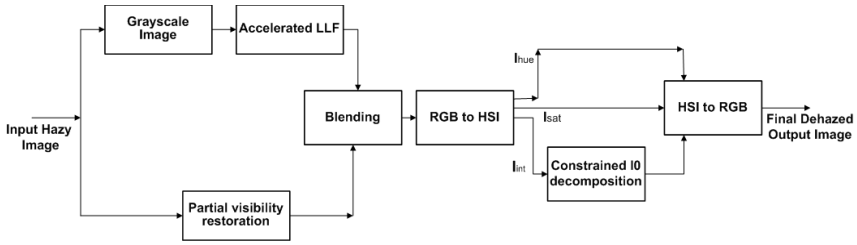

Fig. 1. Proposed technique for haze removal of images.

is required for visual enhancement of the image. For this purpose, constrained gradient l_0 decomposition is used, which is suitable for visually enhancing the images in low-light or dark conditions. This step improves the brightness of the image and makes it visually appealing. The combination of all these steps is used for the development of a simple framework and pipeline for effectively removing haze and restoring the visibility of a degraded hazy image. The proposed technique not only handles the sky problem but also removes the visual artifacts in the dehazed image. The combination of different steps used in our technique is totally unique. The partial visibility of the image is restored by inferring the atmospheric veil using hybrid median filtering. This step is partially based on an idea presented in [7] with the modification of hybrid median filtering. Moreover, the proposed work considers the output obtained after this step as partially restored image instead of a fully dehazed image. The accelerated local Laplacian filtering step applied on the image with partially restored visibility is based on the idea presented in [21]. The constrained gradient decomposition step is somewhat based on the idea presented in [23]. The block diagram of the proposed technique is shown in Fig. 1.

II. Proposed Methodology

The hazy images suffer from different problems which may include low contrast, degraded visual quality, and distorted and inconsistent colors. It is very important but also quite challenging to obtain a haze-free image having a good contrast and enhanced visual quality. The partial visibility of the hazy image is initially restored using extraction of atmospheric veil through a hybrid median filter which has good edge and detail preserving characteristics. However, this method, if used alone for dehazing, may suffer from visible artifacts. Therefore, some other steps are added to remove haze and obtain an image without having dark appearance, color distortion, or visual artifacts. The hazy image is converted to a grayscale, and accelerated local Laplacian filtering [17] is applied to preserve edges and minimizes the visual artifacts. However, some regions in the resulting image appear darker; therefore, the constrained l_0 gradient image decomposition is used to enhance the detail layer using just noticeable difference (JND)-based boosting, while the base layer is enhanced using median-based gamma correction. This step improves the brightness of the image, and makes the images visually appealing.

Let H be the hazy input image having dimensions $A \times B \times \gamma$ where $a = 1, 2, \ldots A$ are rows, $b = 1, 2, \ldots B$ are columns, and $\gamma \in \{\text{Red, Green, Blue}\}$ are color bands. The hazy image is modeled as

$$H^{\gamma}(a,b) = T(a,b)R^{\gamma}(a,b) + (1 - T(a,b))\Lambda \tag{1}$$

where H is the observed hazy image, R is the original (haze free) image, T is the scene transmission, and Λ is the atmospheric light. The target of image dehazing is to recover R, Λ, and $T = e^{-\vartheta d}$, where d represents depth of the scene, and ϑ represents the atmospheric extinction (scattering and absorption) coefficient. The term TR is the direct attenuation, whereas $\Lambda(1 - T)$ is the atmospheric veil V, responsible for inconsistent and distorted colors in the scene. The observed image can be modeled in terms of atmospheric veil as

$$H^{\gamma}(y,z) = R^{\gamma}(a,b)\left(1 - \frac{V(a,b)}{\Lambda}\right) + V(a,b). \tag{2}$$

The first step is the estimation of Λ, for which white balance is applied by making an assumption that Λ is [1, 1, 1] just as in [7]. The next step is to extract the atmospheric veil V. The atmospheric veil inference for obtaining an image with partially restored visibility in our letter is somewhat related to [7]. However, it is different from [7] because the method for inferring the atmospheric veil is different from [7] and the resultant dehazed image obtained is only considered as an image with partially restored visibility, which is passed through various other steps which are not a part of [7]. In the proposed technique, V is inferred by using the hybrid median filter [29] which involves a multistep ranking operation using two subgroups in the vertical, horizontal, and diagonal directions centered on the reference pixel. The median of each subgroup is computed. The filtered output is the median of the medians of these subgroups. In comparison with the basic version of the median filter used in [7], the hybrid median filter has better detail preserving characteristics. Thus, the inferred atmospheric veil V is smooth without the loss of useful edge information.

Let W be the minimum color component of H computed, i.e., $W = \min_{\gamma}(H^{\gamma})$, the hybrid median filtered image is $M = \xi(W)$, where ξ is the filtering operator. The atmospheric veil V is

$$V = \rho \max(\min(O, W), 0) \tag{3}$$

and

$$O = M - \xi|W - M| \tag{4}$$

where $\rho \in [0, 1]$ is a scale factor representing the strength of visibility restoration. After computing the atmospheric veil V and the airlight Λ, $R(a,b)$ can be obtained as

$$R^{\gamma}(a,b) = \frac{H^{\gamma}(a,b) - V(a,b)}{1 - V(a,b)/\Lambda}. \tag{5}$$

The image R contains partial haze and some visual artifacts which are significantly removed using the accelerated local Laplacian filtering. This filter is computationally efficient with

(a) (b) (c) (d) (e) (f)

Fig. 2. Stepwise output. (a) Original image. (b) Partial visibility restoration. (c) Blending. (d) Boosted base layer. (e) Boosted detail layer. (f) Dehazed image.

linear complexity and also reduces the artifacts produced in the filtered image, but some regions in resulting image may still have visual artifacts and low brightness; therefore, further processing is required. So the original hazy image is converted to a grayscale image $\tilde{G}$ using the formula based on International Telecommunication Union standard [22] that is,

$$\tilde{G} = 0.299H^{\text{Red}} + 0.5871H^{\text{Green}} + 0.114H^{\text{Blue}}. \quad (6)$$

The image $\tilde{G}$ is passed through a computationally efficient local Laplacian filter [21] that is,

$$G \xleftarrow[\text{Laplacian Filter}]{\text{Fast Local}} \tilde{G}(\tau, \nu) \quad (7)$$

where τ and ν represent the smoothing factor and the edge amplitude. While this filter has good edge preserving performance and is computationally efficient, however, it darkens some portions of the image [21]. Therefore, constrained l_0 gradient-based image decomposition is used to generate visually plausible results, even in low light. The initial restored image R and G are blended through multiplication to obtain a resultant image $\dot{I}$ that is,

$$\dot{I}^{\gamma} \xleftarrow{\text{Blending}} (G, R^{\gamma}). \quad (8)$$

$\dot{I}$ is converted to HSI colorspace

$$(I^{\text{hue}}, I^{\text{sat}}, I^{\text{int}}) \xleftarrow{\text{RGB to HSI}} \dot{I} \quad (9)$$

and the intensity component I^{int} is then decomposed into a base layer and a detail layer through constrained l_0 gradient image decomposition [23] that is,

$$(I^{\text{Base}} + I^{\text{Detail}}) \xleftarrow{\text{decomposition}} I^{\text{int}}. \quad (10)$$

The HSI color space is closer to human visual system, whereas the constrained l_0 gradient image decomposition enhances the visual quality of the image by enhancing the detail layer I^{Detail} using JND-based boosting, and also enhancing the base layer using median-based gamma correction. This step improves the brightness of the image and makes it visually appealing [23]. The final dehazed image I_{Deh} is

$$I_{\text{Deh}} \xleftarrow{\text{HSI to RGB}} (I^{\text{hue}}, I^{\text{sat}}, I) \quad (11)$$

where I is the enhanced intensity component. Fig. 2 shows the stepwise output of proposed technique.

III. Results and Discussion

The proposed technique is compared with the existing techniques presented in [2], [5], and [15], visually as well as quantitatively. Quantitative analysis is performed using global contrast factor α_{GCF} [27], standard deviation α_S [15], edge intensity α_{EI} [15], normalized absolute error α_{NAE} [28], structural similarity index (SSIM) [24], and two no-reference image quality metrics, namely, naturalness image quality evaluator α_{NIQ} [25] and blind/referenceless image spatial quality evaluator α_{BR} [26]. Higher values of α_{GCF}, α_S, and α_{EI} indicate SSIM, whereas lower values of α_{NAE}, α_{NIQ}, and α_{BR} indicate better results. The simulations were performed on Intel Core i5 with 4 GB RAM.

In [2], the airlight was estimated using 0.1% brightest pixels in the dark channel while the patch size was taken as 15×15. If the patch size chosen is too small, the restored radiance is oversaturated; on the other hand, if the patch size is chosen to be too large, the halos near edges can become prominent, so this selected patch size was found to have a reasonable dehazing performance for a variety of images. In [5], $C_0 = 30$ and $C_1 = 300$, window size was 15×15, $\lambda = 2$, $\beta \in [1, 2^8]$, and the maximum value of each color channel was taken as an estimate of airlight. The details of these parameters can be found in the "Experimental Results" section in [5]. In [15], a value of 1.5 was selected as a regularization parameter, 15×15 as window size, $\beta \in [1, 2^8]$, and the boundary constraints were made adaptive through an empirical formula. For the proposed technique, the parameters s_v, $s_{\max}$, and p were chosen as 41, 1, and 0.8, respectively (described in [7]). The scale factor can have values between 0 and 1, as calculated in [7], and an optimal value of 0.8 was selected based on extensive experimentation with outdoor as well as remotely sensed images. For edge preserving constrained gradient decomposition, $s = 0.7$, $\lambda = 0.001$, $\beta = 0.02$, and $\sigma = 0.015$ were selected through multiple experiments. The threshold values for first differential of Gaussian and edge map were selected as 0.75 and 0.2, respectively. For JND boosting, μ was set to 4.

Fig. 3 presents the visual comparison of these techniques on two remotely sensed images. Example 1 is the satellite image (1024×694 pixels) of Chiapa de Corzo captured on May 19, 2010, by Earth Observatory NASA. The camera type was multispectral scanner. Example 2 is the aerial view of Willard, Ohio (1280×960 pixels), captured on September 12, 2012, using Canon Powershot SX 130 IS. In Example 1, haze is partially removed in the images generated by the techniques in [2], [5], and [15] and the colors are distorted, while the image produced by the proposed technique is haze free, visually appealing, and has correctly restored colors. Example 2 shows that the images dehazed in [2], [5], and [15] have dark appearance and distorted colors, whereas the proposed technique dehazes the image without making it dark or having distorted colors.

In Fig. 4, in Example 3, the proposed technique has dehazed the background region behind the tree more effectively as compared to that in [2], [5], [15], and [19]. In Example 4, the dehazing performance of the proposed technique is better than that in [19], especially in the small distant building and object adjacent to the large buildings in our image, which are not clearly visible in the image dehazed in [19], whereas the images dehazed in [2], [5], and [15] suffer from distorted colors and artifacts. It can be seen in Fig. 5 that the proposed

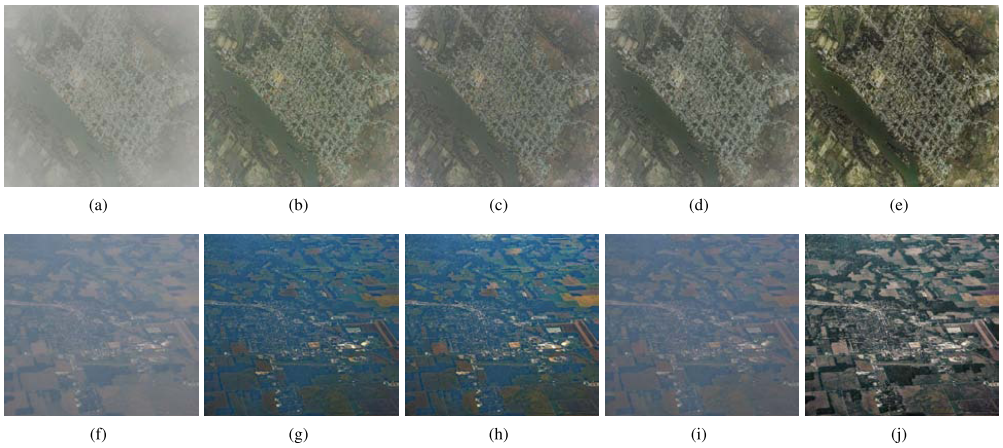

Fig. 3. Examples 1 and 2. (a) and (f) Original image. (b) and (g) He *et al.*'s technique [2]. (c) and (h) Meng *et al.*'s technique [5]. (d) and (i) Baig *et al.*'s technique [15]. (e) and (j) Proposed technique.

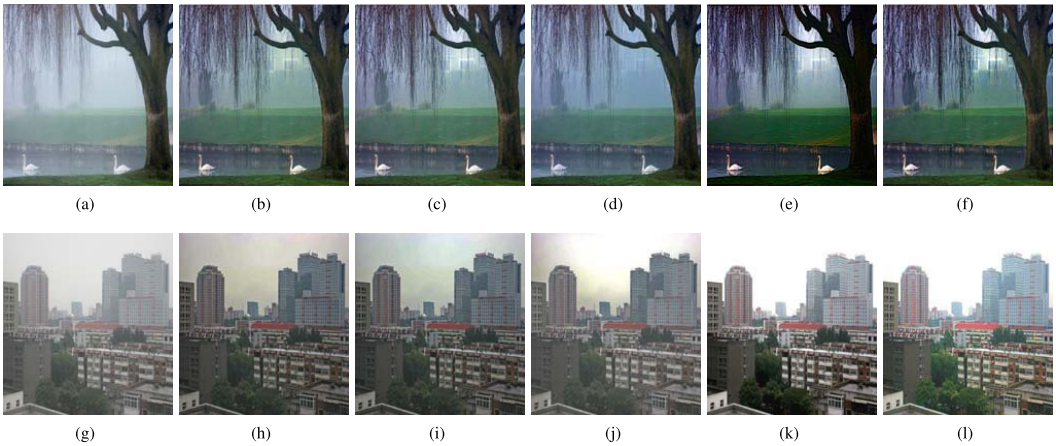

Fig. 4. Examples 3 and 4. (a) and (g) Original image. (b) and (h) He *et al.*'s technique [2]. (c) and (i) Meng *et al.*'s technique [5]. (d) and (j) Baig *et al.*'s technique [15]. (e) and (k) Wang *et al.*'s technique [19]. (f) and (l) Proposed technique.

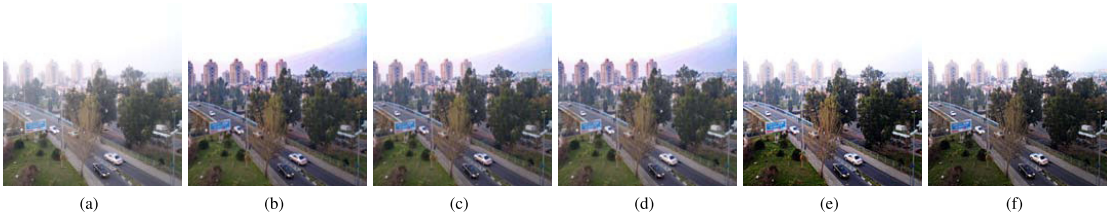

Fig. 5. Example 5. (a) Original image. (b) He *et al.*'s technique [2]. (c) Meng *et al.*'s technique [5]. (d) Baig *et al.*'s technique [15]. (e) Kaplan *et al.*'s technique [18]. (f) Proposed technique.

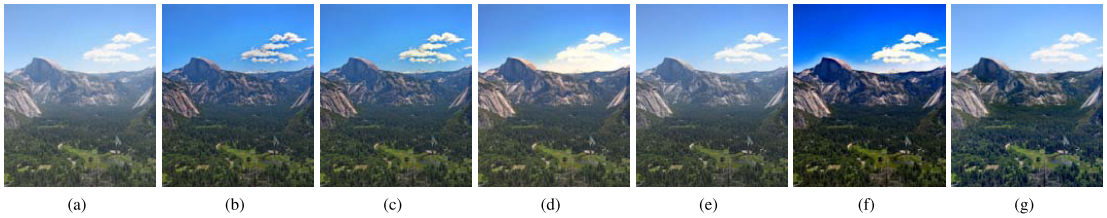

Fig. 6. Example 6. (a) Original image. (b) He *et al.*'s technique [2]. (c) Meng *et al.*'s technique [5]. (d) Baig *et al.*'s technique [15]. (e) Kaplan *et al.*'s technique [18]. (f) Wang *et al.*'s technique [19]. (g) Proposed technique.

technique has dehazed all areas including the buildings and trees effectively, whereas visible artifacts in the sky region are present in the images dehazed in [2], [5], and [15]. In Fig. 6, the image dehazed in [18] still contains some haze in the distant regions, whereas the image dehazed in [19] suffers from color distortion at the top of the mountain, and the clouds and sky region. The image generated in [15] has distorted colors and visible haze below the clouds. The proposed technique has removed haze from the near as well as the distant regions without distorting the colors. Table I presents

TABLE I
QUANTITATIVE COMPARISON

Techniques	SSIM	α_{GCF}	α_S	α_{EI}	α_{NAE}	α_{NIQ}	α_{BR}
Example 1							
He et al. [2]	0.7596	3.8127	0.1503	0.5276	0.2847	6.3063	44.5047
Meng et al. [5]	0.7325	3.5071	0.1599	0.5873	0.2729	6.2420	43.3747
Baig et al. [15]	0.7948	3.8127	0.1480	0.4692	0.2842	**4.2099**	36.1182
Proposed	**0.8512**	**5.9674**	**0.1654**	**0.5911**	**0.2343**	4.5078	**35.3087**
Example 2							
He et al. [2]	0.6686	4.3501	0.1186	0.2282	0.3697	3.1290	30.1861
Meng et al. [5]	0.6377	4.2054	0.0873	0.2180	0.3355	3.1538	30.6030
Baig et al. [15]	0.8592	2.0651	0.0661	0.1162	0.1610	4.6939	40.4252
Proposed	**0.8948**	**4.5865**	**0.1371**	**0.2813**	**0.1194**	**3.0714**	**30.1059**
Example 3							
He et al. [2]	0.8271	5.9130	0.1894	0.2885	0.2970	3.8972	35.7959
Meng et al. [5]	0.8368	6.0526	0.2002	0.2987	0.2886	3.8424	35.8465
Baig et al. [15]	0.8715	5.6010	0.1954	0.2328	0.2836	3.9304	32.7989
Wang et al. [19]	0.5963	6.9065	0.2428	0.3769	0.5116	4.0237	42.2394
Proposed	**0.8733**	**6.9920**	**0.2518**	**0.3794**	**0.2325**	**3.7509**	**32.6178**
Example 4							
He et al. [2]	0.7917	5.0949	0.2199	0.2470	0.2547	3.3024	**22.5977**
Meng et al. [5]	0.8028	5.0767	0.2282	0.2491	0.2468	3.2533	22.7738
Baig et al. [15]	0.8294	4.5326	0.2392	0.2155	0.1048	3.4573	24.4253
Wang et al. [19]	0.8334	7.0476	0.2258	0.3044	0.1826	3.8710	38.1830
Proposed	**0.8409**	**7.1998**	**0.2895**	**0.3154**	**0.1039**	**3.2136**	23.0256
Example 5							
He et al. [2]	0.8586	6.1096	0.3319	0.2130	0.1629	3.4131	13.5999
Meng et al. [5]	0.9024	5.7882	0.3236	0.1987	0.1286	5.2368	13.1187
Baig et al. [15]	0.9006	5.7110	0.3118	0.1997	0.1131	5.2288	13.3070
Kaplan et al. [18]	0.7845	7.1185	0.3727	0.2773	0.1627	9.4445	23.3470
Proposed	**0.9066**	**7.5293**	**0.3767**	**0.2813**	**0.1127**	**5.0891**	**13.0716**
Example 6							
He et al. [2]	0.8421	5.0665	0.2532	0.2304	0.3662	2.5487	10.6996
Meng et al. [5]	0.8609	5.0388	0.2523	0.2270	0.2654	2.4864	9.8325
Baig et al. [15]	0.8678	5.1893	0.2687	0.2199	0.1551	2.3664	8.9220
Kaplan et al. [18]	0.8213	4.9051	0.2652	0.2841	0.1236	3.1050	11.3786
Wang et al. [19]	0.6558	**8.1525**	0.2825	0.2667	0.4407	2.4876	9.7591
Proposed	**0.8996**	7.2126	**0.2844**	**0.2851**	**0.1205**	**2.3362**	**8.0972**

the quantitative comparison of the proposed technique and the state-of-the-art existing techniques. It can be observed that the proposed technique provides overall better metric values.

IV. CONCLUSION

An effective framework for dehazing and visibility restoration of outdoor as well as remotely sensed RGB images is presented. For initial dehazing, the framework makes use of hybrid median filtering, as well as the fast local Laplacian filtering for preserving the details. For improving the brightness, l_0 gradient-based image decomposition is utilized. The comparison results of the proposed technique with existing dehazing techniques show that the proposed technique handles the sky regions in images better than existing techniques. Moreover, it is effective in producing dehazed images with preserved color information of the original scene and the fine image details.

REFERENCES

[1] R. Fattal, "Single image dehazing," *ACM Trans. Graph.*, vol. 27, no. 3, 2008, Art. no. 72.

[2] K. He, J. Sun, and X. Tang, "Single image haze removal using dark channel prior," *IEEE Trans. Pattern Anal. Mach. Intell.*, vol. 33, no. 12, pp. 2341–2353, Dec. 2011.

[3] Q. Zhu, J. Mai, and L. Shao, "Single image dehazing using color attenuation prior," in *Proc. Brit. Mach. Vis. Conf.*, Sep. 2014, pp. 1–10.

[4] X. Zhu, Y. Li, and Y. Qiao, "Fast single image dehazing through Edge-Guided Interpolated Filter," in *Proc. 14th IAPR Int. Conf. Mach. Vis. Appl.*, Tokyo, Japan, May 2015, pp. 18–22.

[5] G. Meng, Y. Wang, J. Duan, S. Xiang, and C. Pan, "Efficient image dehazing with boundary constraint and contextual regularization," in *Proc. IEEE Int. Conf. Comput. Vis.*, Sydney, NSW, Australia, Dec. 2013, pp. 1–8.

[6] Y.-H. Lai, Y.-L. Chen, C.-J. Chiou, and C.-T. Hsu, "Single-image dehazing via optimal transmission map under scene priors," *IEEE Trans. Circuit System Video Technol.*, vol. 25, no. 1, pp. 1–14, Jan. 2015.

[7] J.-P. Tarel and N. Hautière, "Fast visibility restoration from a single color or gray level image," in *Proc. IEEE 12th Int. Conf. Comput. Vis.*, Kyoto, Japan, Sep./Oct. 2009, pp. 2201–2208.

[8] J. Long, Z. Shi, W. Tang, and C. Zhang, "Single remote sensing image dehazing," *IEEE Geosci. Remote Sens. Lett.*, vol. 11, no. 1, pp. 59–63, Jan. 2014.

[9] C. Ancuti and C. O. Ancuti, "Effective contrast-based dehazing for robust image matching," *IEEE Geosci. Remote Sens. Lett.*, vol. 11, no. 11, pp. 1871–1875, Nov. 2014.

[10] A. Makarau, R. Richter, R. Müller, and P. Reinartz, "Haze detection and removal in remotely sensed multispectral imagery," *IEEE Trans. Geosci. Remote Sens.*, vol. 52, no. 9, pp. 5895–5905, Sep. 2014.

[11] A. Makarau, R. Richter, D. Schläpfer, and P. Reinartz, "Combined haze and cirrus removal for multispectral imagery," *IEEE Geosci. Remote Sens. Lett.*, vol. 13, no. 3, pp. 379–383, Mar. 2016.

[12] J. Lüthen, J. Wörmann, M. Kleinsteuber, and J. Steurer, "A RGB/NIR data set for evaluating dehazing algorithms," *Electron. Imag.*, vol. 2017, no. 12, pp. 79–87, Jan. 2017.

[13] W. Wencheng, X. Yuan, X. Wu, and Y. Liu, "Fast image dehazing method based on linear transformation," *IEEE Trans. Multimedia*, vol. 19, no. 6, pp. 1142–1155, Jun. 2017.

[14] L. Zhigang, G. Fan, J. Gong, Y. Wang, and X. Lu, "Perception oriented transmission estimation for high quality image dehazing," *Neurocomputing*, vol. 224, pp. 82–95, Feb. 2017.

[15] N. Baig, M. M. Riaz, A. Ghafoor, and A. M. Siddiqui, "Image dehazing using quadtree decomposition and entropy-based contextual regularization," *IEEE Signal Process. Lett.*, vol. 23, no. 6, pp. 853–857, Jun. 2016.

[16] D. Singh and V. Kumar, "Modified gain intervention filter based dehazing technique," *J. Modern Opt.*, vol. 64, no. 20, pp. 2165–2178, 2017.

[17] D. Singh and V. Kumar, "Dehazing of remote sensing images using improved restoration model based dark channel prior," *Imag. Sci. J.*, vol. 65, no. 5, pp. 282–292, 2017.

[18] N. H. Kaplan, K. K. Ayten, and A. Dumlu, "Single image dehazing based on multiscale product prior and application to vision control," *Signal Image Video Process.*, vol. 11, no. 8, pp. 1389–1396, 2017.

[19] J. Wang, K. Lu, J. Xue, N. He, and L. Shao, "Single image dehazing based on the physical model and MSRCR algorithm," *IEEE Trans. Circuits Syst. Video Technol.*, Jul. 2017.

[20] W. Ni, X. Gao, and Y. Wang, "Single satellite image dehazing via linear intensity transformation and local property analysis," *Neurocomputing*, vol. 175, pp. 25–39, Jan. 2016.

[21] M. Aubury, S. Paris, S. W. Hasinoff, J. Kautz, and F. Durand, "Fast local Laplacian filters: Theory and applications," *ACM Trans. Graph.*, vol. 33, no. 5, 2014, Art. no. 167.

[22] J. Gomes and L. Velho, *Image Processing for Computer Graphics and Vision*. London, U.K.: Springer-Verlag, 2013.

[23] S.-C. Pei, C.-T. Shen, and T.-Y. Lee, "Visual enhancement using constrained L0 gradient image decomposition for low backlight diplays," *IEEE Signal Process. Lett.*, vol. 19, no. 12, pp. 183–186, Dec. 2012.

[24] Z. Wang, A. C. Bovik, H. R. Sheikh, and E. P. Simoncelli, "Image quality assessment: From error visibility to structural similarity," *IEEE Trans. Image Process.*, vol. 13, no. 4, pp. 600–612, Apr. 2004.

[25] A. Mittal, R. Soundararajan, and A. C. Bovik, "Making a 'completely blind' image quality analyzer," *IEEE Signal Process. Lett.*, vol. 20, no. 3, pp. 209–212, Mar. 2013.

[26] A. Mittal, A. K. Moorthy, and A. C. Bovik, "No-reference image quality assessment in the spatial domain," *IEEE Trans. Image Process.*, vol. 21, no. 12, pp. 4695–4708, Dec. 2012.

[27] K. Matković, L. Neumann, A. Neumann, T. Psik, and W. Purgathofer, "Global contrast factor-a new approach to image contrast," in *Proc. Comput. Aesthetics Graph., Vis. Imag.*, Girona, Spain, May 2005, pp. 1–9.

[28] V. Santhi, D. Acharjya, and M. Ezhilarasan, *Emerging Technologies in Intelligent Applications for Image and Video Processing*. Hershey, PA, USA: IGI Global, 2016.

[29] E. R. Davies, *Machine Vision: Theory, Algorithms, Practicalities*. Amsterdam, The Netherlands: Elsevier, 2006.